JOURNAL OF SOLID STATE CHEMISTRY 42, 47–74 (1982)

Electron Beam-Induced Reduction of Higher Oxides of the Rare Earths: A High-Resolution Electron Microscopic Study

H. A. EICK, L. EYRING,* E. SUMMERVILLE, AND R. T. TUENGE

Department of Chemistry and the Center for Solid State Science, Arizona State University, Tempe, Arizona 85287

Received November 30, 1981

Many compounds are unstable in the beam of the electron microscope or can be made so by increasing the beam intensity. Observations of beam-induced decompositions of the higher oxides of the rare earths were made under circumstances where the details of reduction in the vacuum of the microscope can be examined. The ζ and ι phases of praseodymium oxide (Pr_9O_{16}, Pr_7O_{12}) and the ι phase of terbium oxide were observed to reduce directly to the ϕ phase (R_2O_3), revealing the texture of intermediate stages of the reaction. The nature of the ZrO_2–Sc_2O_3 system in the same intermediate composition region is also revealed and compared to the binary rare earth systems. Particular attention is paid to the appearance of composite crystals in these semicoherent phases during reaction. From these varied observations speculations on the mechanism of the decomposition are presented.

Introduction

It is of interest to describe the mechanism of solid-state reactions and transformations at the atomic level. An instrument of exceptional power for this purpose is the high-resolution transmission electron microscope (HRTEM) (*1–3*). With this instrument selected area electron diffraction and structure imaging can provide a two-dimensional representation of a structure, including defects, undergoing reaction at a point-to-point resolution of from 2 to 3.5 Å. With the aid of image calculations the contrast of the micrographs can be interpreted in terms of the positions of the atoms (*1, 4, 5*). This technique has been applied to a structural study of the fluorite-related homologous series of intermediate phases in the rare earth oxide systems (*6–9*).

Any of the higher oxides of praseodymium or terbium are easily reduced to the *C*-type fluorite-related sesquioxides. High-resolution images of the [111] zone of these have been published (*10*), together with references to discussions of their structural relationship with the *A*- and *B*-type rare earth sesquioxides. The higher oxides (R_nO_{2n-2}, $4 \leq n \leq \infty$) belong either to an even or an odd n series (*6*) and for $n \geq 7$ the members in each series are structurally closely related. They have planes in common at different spacings containing six-coordinated metal atoms. The sesquioxide ($n = 4$) is compositionally one of the series but, although it is cubic and fluorite related, when formed from the higher oxides it requires a more profound structural rearrangement of the oxygen sublattice than that which occurs between the members of the odd and even series. Since the reduction is accomplished in the vacuum of the microscope with moderate beam heating, it

* Author to whom correspondence should be addressed.

0022-4596/82/040047-28$02.00/0

is possible to observe the reaction directly as it proceeds.

In this paper we shall discuss the beam-induced vacuum reduction of the higher oxides Pr_7O_{12} (ι phase) and Pr_9O_{16} (ζ phase) to the *C*-type sesquioxide (R_4O_6, ϕ phase) or to an oxygen-rich *C*-type phase ($R_4O_{6+\delta}$) called σ. *R* refers to Pr, Tb, or (Zr, Sc). These lower oxides ϕ (*C* type) and σ phases are both bixbyite-type structures; the latter with an oxygen excess. Whereas most structural studies of solid-state reactions are made on bulk samples using X-ray diffraction techniques, the methods of HRTEM afford a more intimate examination of the changes that occur at the atomic level.

Experimental

Crystalline samples of the ζ and ι phases were prepared by the hydrothermal methods previously described (*11*). The crystals were ground in an agate mortar under liquid nitrogen. An acetone slurry of the pulverized material was placed on a holey carbon microscope grid. The small crystal fragments were examined with a JEM 100B transmission electron microscope operated at 100 kV using a technique that has been previously described (*12*). Both selected area electron diffraction and lattice images were utilized in the study.

Because of the ease of reduction of the samples under imaging conditions, appreciable reaction could occur unless care was taken during the acquisition of a through-focus series of images. Beam irradiation to induce phase reaction was achieved either by concentrating the beam with the second condenser current control (mild heating) or by removing the condenser aperture briefly (intense heating). The level of radiation was selected as required to achieve the desired product.

Since the lanthanide oxide intermediate phases are most advantageously observed and compared in the $\langle 211 \rangle_F$ and $\langle 111 \rangle_F$ zones of the parent fluorite, only these zones were examined in detail. Distances on the electron diffraction patterns were converted to reciprocal lattice spacings by comparison with the interplanar spacings calculated previously for these structures (*6*). Measured lattice image fringe spacings were converted to direct lattice vectors by applying the known magnification factor of 5×10^5 to the original micrograph. Selected image photographs in which excessive interferences resulted from overlap of phases were examined by optical diffraction to obtain phase identification. The particular oxide phases present in the crystal, both at the start of the reaction and as the process advanced, could be readily identified in the fluorite zone chosen for study by their distinctive electron diffraction patterns and by their characteristic lattice images (*4, 6–9*).

Specimens of $Zr_ySc_{1-y}O_x$ prepared for this study were mixtures of ZrO_2 and Sc_2O_3 of desired ratios arc-melted on a water-cooled copper hearth using a tungsten electrode under an argon atmosphere.

Results and Discussion

The Pseudobinary System ZrO_2–Sc_2O_3 with High Sc_2O_3 Content

The pseudobinary phase $Zr_3Sc_4O_{12}$ is isostructural with ι phase Pr_7O_{12} and Tb_7O_{12} (*14*), with the Zr and Sc atoms occupying the rare earth atom positions at random (*13*). Sc_2O_3 has the *C*-type rare earth sesquioxide structure isostructural with the ϕ phase Pr_2O_3 and Tb_2O_3. Figure 1 shows a series of $\langle 111 \rangle_F$ zone images of crystals from an arc-melted specimen with a composition of approximately $Zr_{0.29}Sc_{0.71}O_{1.64}$. At this composition the sample should consist of about one-third *C*-type sesquioxide and two-thirds $Zr_3Sc_4O_{12}$. As shown in Fig. 1, the sample consists of domains of *C* type

embedded in an ι-phase matrix. The images can be interpreted directly even in the overlay regions and regardless of the location of the domain within the sample (i.e., whether the C type occurs superficially or internally). Figure 2a shows a typical diffraction pattern from such a sample with many unallowed reflections resulting from dynamical interaction of ι-phase reflections with those of C type. Figure 2b illustrates a constructed overlay of the two phases from their individual images. This image, like that of an overlay of the two twin orientations of ι (*4*), is independent of the choice of origin. Figure 1b has inverted contrast relative to Fig. 1a due to a change of defocus. It is interesting that even such a potentially complex image has good contrast and can be interpreted directly. Many of the images show ill-defined regions which appear to result from the presence of a trace of C type, as if incipient phase separation had resulted in a thin layer of C-type material with the ι phase. This feature is also seen during reduction of Pr_7O_{12} and Tb_7O_{12}, as discussed later. Probably all stages from small (100-Å diameter) crystallites to single unit cells of Sc_2O_3 are present in a matrix of $Zr_3Sc_4O_{12}$. On annealing the sample at 1600°C for 28 hr, macroscopic phase separation occurred and few ι-C-type boundaries were observed. Figure 3 shows one of the few boundaries observed. This $\langle 211 \rangle_F$ zone image shows Sc_2O_3 on the left, ι on the right with a diffuse, inclined boundary region which is an overlay image of ι, and C type separating them. The ambiguities of equilibrium in ternary systems of this type have recently been discussed in some detail (*15*).

In this pseudobinary system, the oxygen content is determined by the ratio of the oxides of fixed valence initially present. In the praseodymium and terbium oxides, on the other hand, the ι phase can be reduced to the ϕ phase, as discussed in the next section.

The Reduction of ι (R_7O_{12}, R = Pr, Tb) to ϕ (R_2O_3) in the Microscope

Many instances of reduction of ι to ϕ in the microscope have been observed. These are summarized here with several illustrations. A general statement can be made that no intermediate phase between $n = 7$ and $n = 4$ has definitely been observed. There were several cases where highly oxidized materials were heated in the microscope and a phase with a multiplicity of six was observed in the electron diffraction pattern but in each case it appeared to be a zone of an $n = 12$ oxide even though the circumstances of its appearance suggested that the composition should have been less than $R_{12}O_{22}$.

Under an oxygen partial pressure of 10^{-7} Torr it is expected that all of the phases with oxygen-to-metal ratios greater than 1.50 can be easily reduced by beam-heating. In fact, such reduction was both a curse and a blessing. It was therefore a little surprising to find that some regions actually oxidized when beam-heated. Many such cases are well documented, with observations both in diffraction and imaging modes.

It now appears that this apparent oxidation is a local effect produced by chemically pumping oxygen from a thicker, hotter part of the crystal. The equilibrium oxygen pressure is therefore higher in these areas and oxygen is pumped to the cooler edges of the crystal. Since the edges are the regions from which both diffraction patterns and images are obtained, it is only the localized oxidation which is observed, although the sample overall is undergoing reduction. One such edge of a PrO_x crystal was seen to undergo the series of transformations

$$\iota(7) \rightarrow \beta(12) \rightarrow \epsilon(10) \rightarrow \epsilon(10) + \beta(12) \rightarrow \text{LPSS} \rightarrow \zeta(9) \rightarrow \epsilon(10),$$

where LPSS is a long-period superstructure with the spots always present as satellite

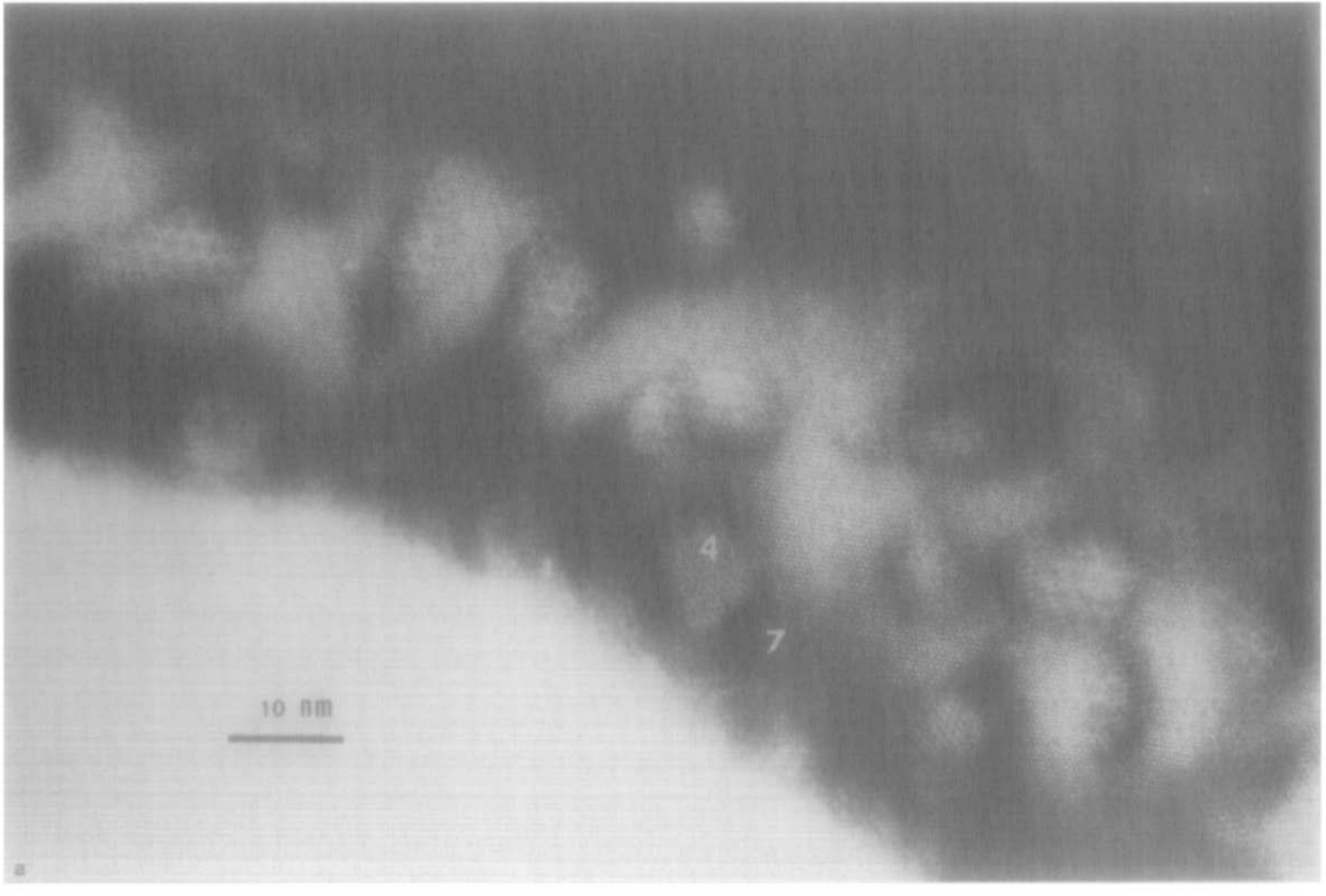

FIG. 1. Domains of Sc_2O_3 (marked 4) in a matrix of $Zr_3Sc_4O_{12}$ (marked 7) as seen in $\langle 111 \rangle_F$ images. FIG 1a. Note the rather regular size of the domains of Sc_2O_3 in a continuous matrix.

FIG. 1b. Note the marked hexagonal array of broad spots (marked A) which result from an overlay of the two phases.

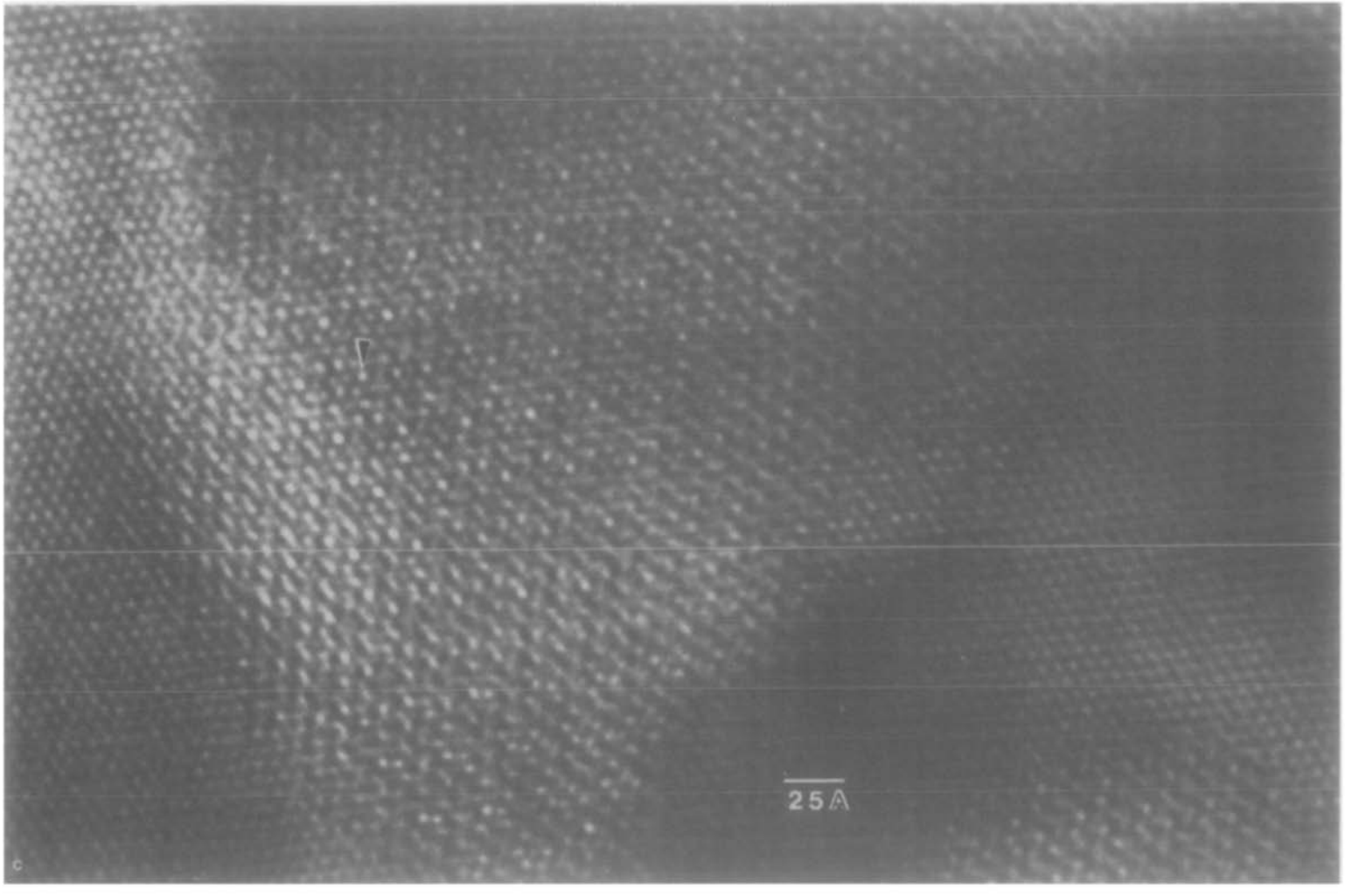

FIG. 1c. An enlarged image of an overlay region showing the irregular patterns which result. The spot marked with an arrow corresponds to the largest spots of Fig. 2b.

pairs, and the number in parentheses is n in R_nO_{2n-2}. On successive heatings the oxygen content of the crystal edge obviously fluctuated erratically, indicating that oxygen was sometimes pumped into the edge faster than it was expelled and sometimes the reverse. With each composition change the crystal reordered. Most often, however, these erratic fluctuations did not arise and a unidirectional reaction occurred.

The environment of the microscope is hostile to any of the higher oxides being studied. However, these compositional changes were induced under conditions more severe than those generally used in this type of study. Nevertheless, such processes were probably occurring to some extent in all crystals of the higher oxides examined. Specimen behavior generally fell into two categories: those which showed no disorder and were extremely unreactive, virtually independent of their constitution, and those which were initially disordered and extremely reactive. Almost invariably the particular fluorite zone of the specimen before reaction was preserved in the change. A new set of superstructure spots heralded the reaction.

Now to continue our discussion of the redution of ι phase by beam-heating. Selected area electron diffraction patterns (SAED) of R_7O_{12} are observed to fade as those of R_2O_3 increase in intensity until only reflections from ϕ phase remain as a strong pattern. At the same time good images of R_7O_{12} become disordered (reduced) and the nuclei of R_2O_3 appear and grow rather isotropically, impinging on each other to give a mosaic of R_2O_3 domains which reflect a rather regular nucleation in the parent phase. There are some apparent exceptions which will be illustrated.

The final result of this general sequence of events is illustrated in Fig. 4. In this case, a crystal of irradiated Pr_7O_{12} yields SAED patterns in the sequence Figs. 4a, b, c and d, in which the superstructure spots characteristic of Pr_7O_{12} dominate the pattern in Fig. 4a and are virtually absent in Fig. 4d, while the reverse is true for the ϕ phase. SAED patterns in Figs. 4b and c, where the phases have more nearly the same degree of scattering, show interesting dynamical effects. Figure 4c, for example, shows scattering of the diffracted beams from ϕ and ι and vice versa, yielding a multiplicity of 7 between spots from $n = 4$ and a multiplicity of 4 between spots from $n = 7$. The image in Fig. 4e is of a thin region of the crystal in the early stages of the overall reduction but where the reaction is locally almost complete. It was taken between the diffraction patterns shown in Figs. 4a and b.

If one considers a projection of the fluorite structure along the threefold $[111]_F$ axis, the metal atoms project as columns in a hexagonal array. The $[111]_F$ is also a threefold axis in both the ι and ϕ phases, but the spacings are different. The ι and ϕ phases are shown superimposed on $[111]_F$ in Fig. 2b. In this figure the large solid circles represent the occurrence of register of the threefold axes in the three structures based upon the origins chosen. A study of this figure will reveal that the ϕ phase can nucleate in an ι matrix in four—and only four—distinct ways to yield an array of image spots where the pattern is shifted one-fourth the spacing of the hexagonal array of the C-type phase (see arrows).

If the ϕ phase were to nucleate in ι at intervals of about 200 Å and if these nuclei were to grow until the reaction was nearly complete, the mosaic pattern of the image illustrated in Fig. 4e would result. Notice that homogeneous regions of about 100 Å in extent are misfit at their boundaries (antiphase boundaries) by $\pm\frac{1}{4}$ or $\frac{1}{2}$ the spacing of the spots correlating with different atom rows in the fluorite subcell. This gives a wavy appearance to the rows of spots when viewed at a low angle to the figure (i.e., parallel to the straight line).

If one observes the same reaction in the

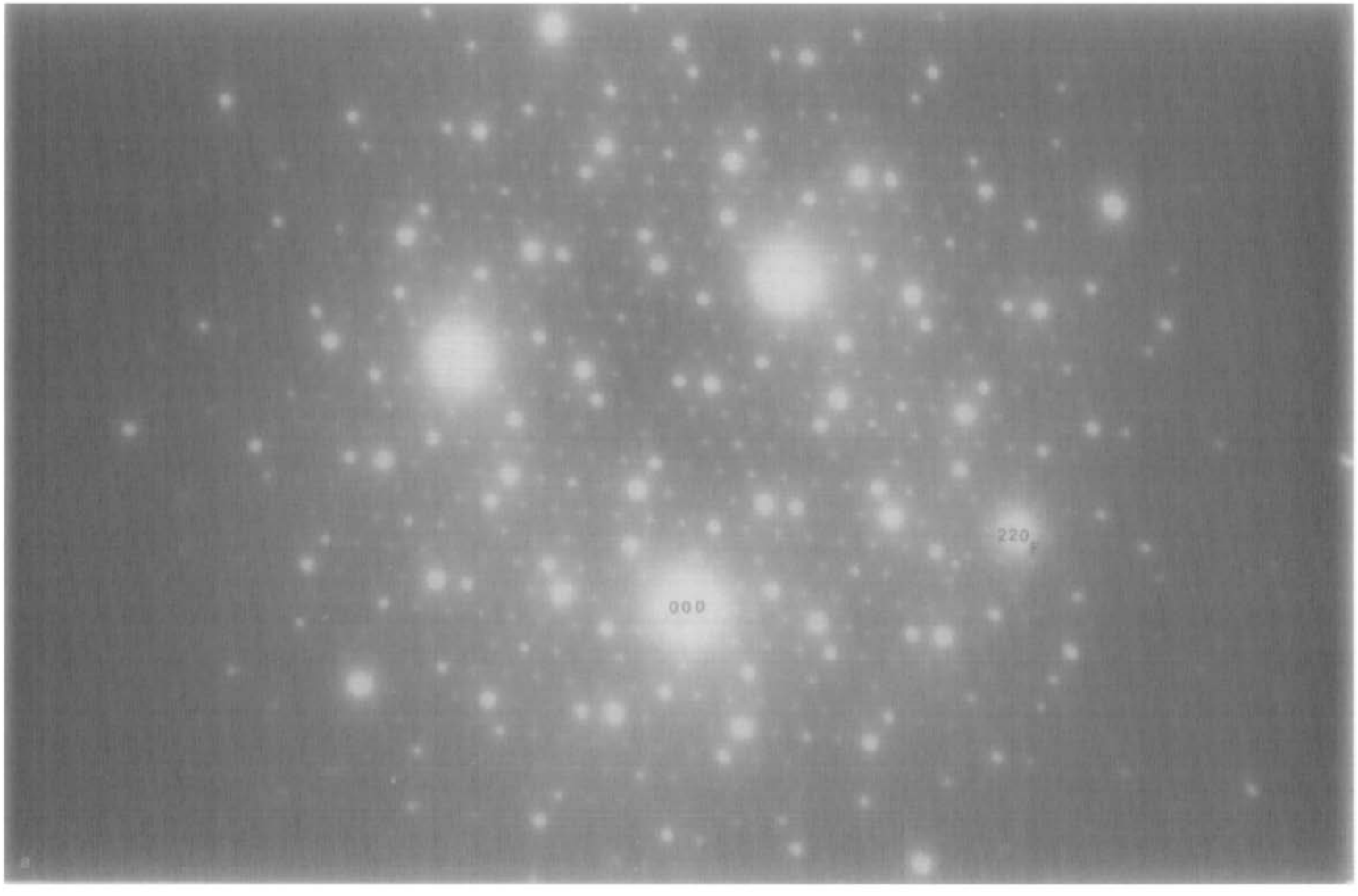

FIG. 2a. Diffraction pattern from a sample imaged in Fig. 1 showing double diffraction effects.

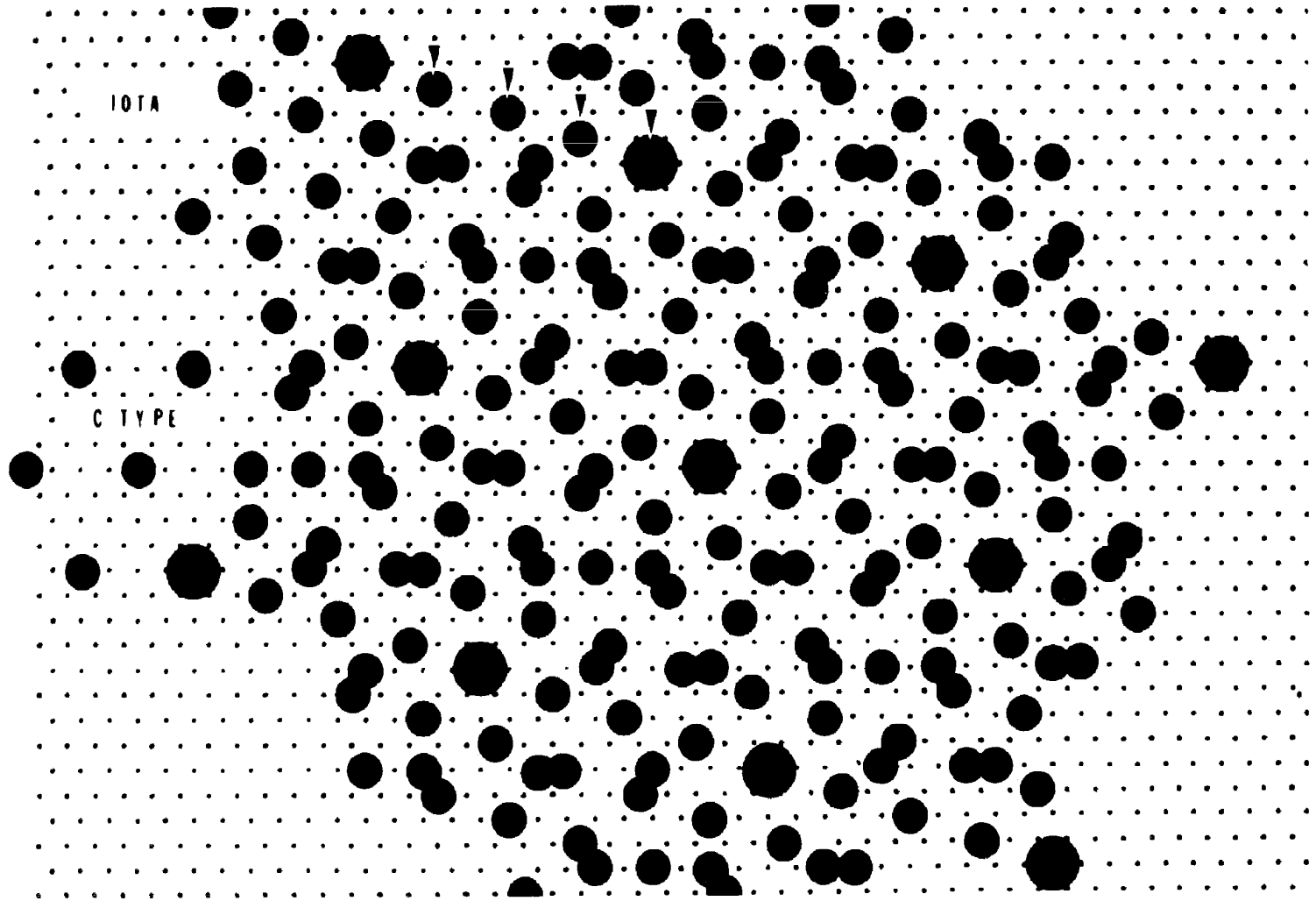

FIG. 2b. Diagram showing the structural basis of an overlay image of *C* type and *ι* from a $\langle 111 \rangle_F$ zone. The arrows designate alternative nucleation sites which would yield a shift of the image spots by $\pm\frac{1}{4}$ or $\frac{1}{2}$.

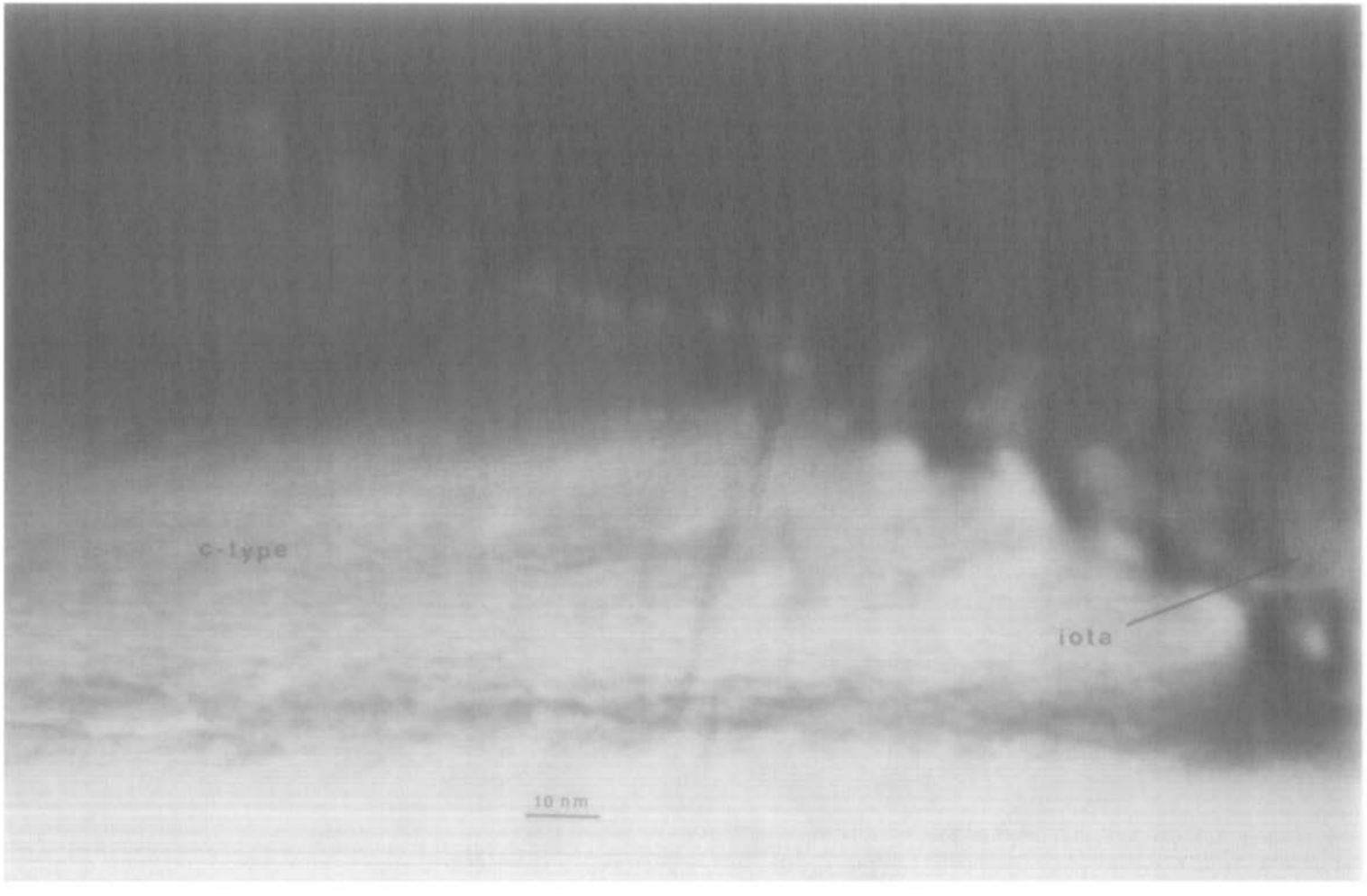

FIG. 3. Regions of C- type and ι phases in an annealed sample of $Zr_{0.29}Sc_{0.71}O_{1.64}$.

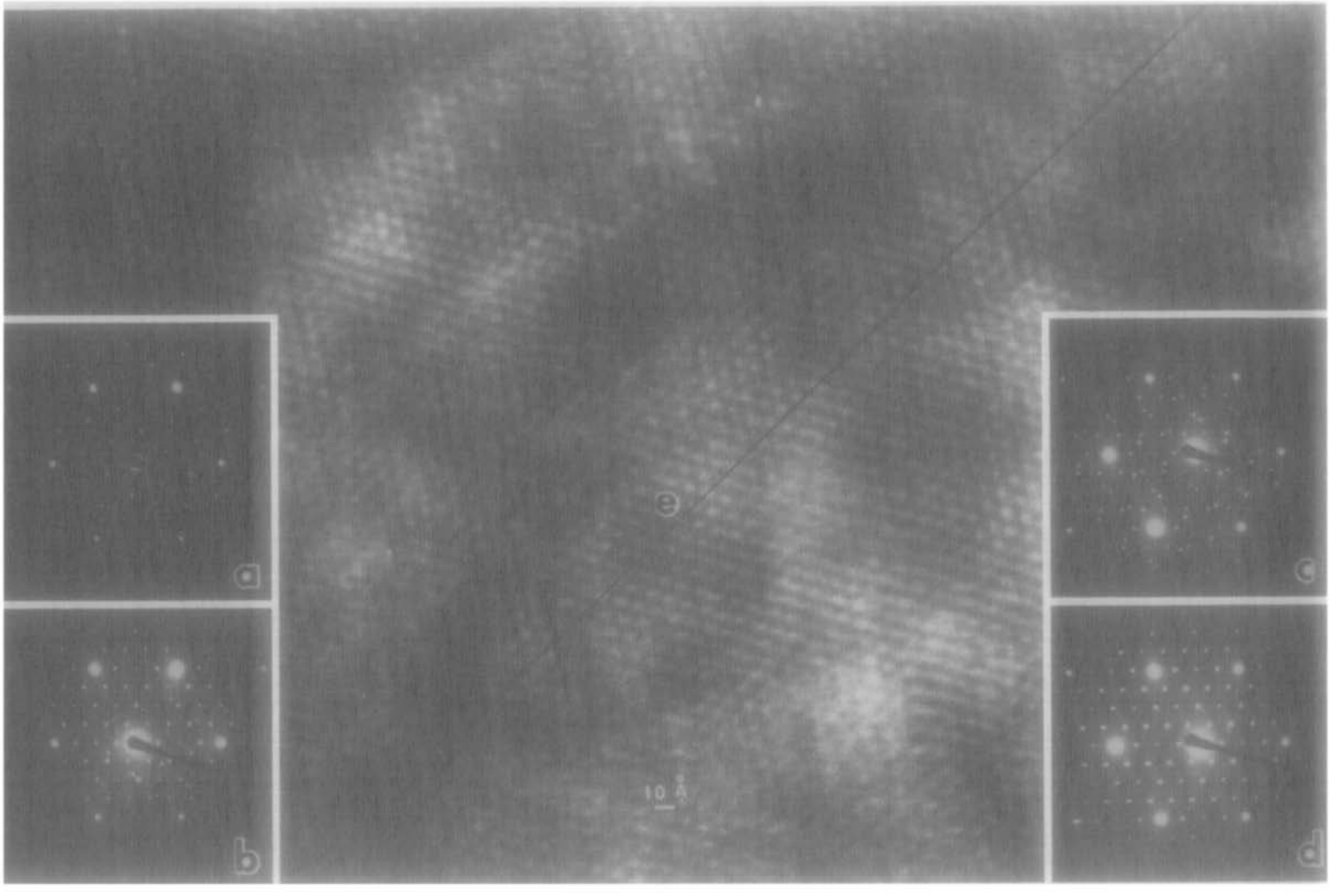

FIG. 4. A region of incomplete reduction of Pr_7O_{12} to Pr_2O_3, $[111]_F$ zone. Inset diffraction patterns marked (a), (b), (c), and (d) show the progress of the reaction. The image (e) was taken between diffraction patterns (a) and (b). The straight line in (e) illustrates shifts of $\pm\frac{1}{4}$ or $\frac{1}{2}$ of the spacing as described in the text.

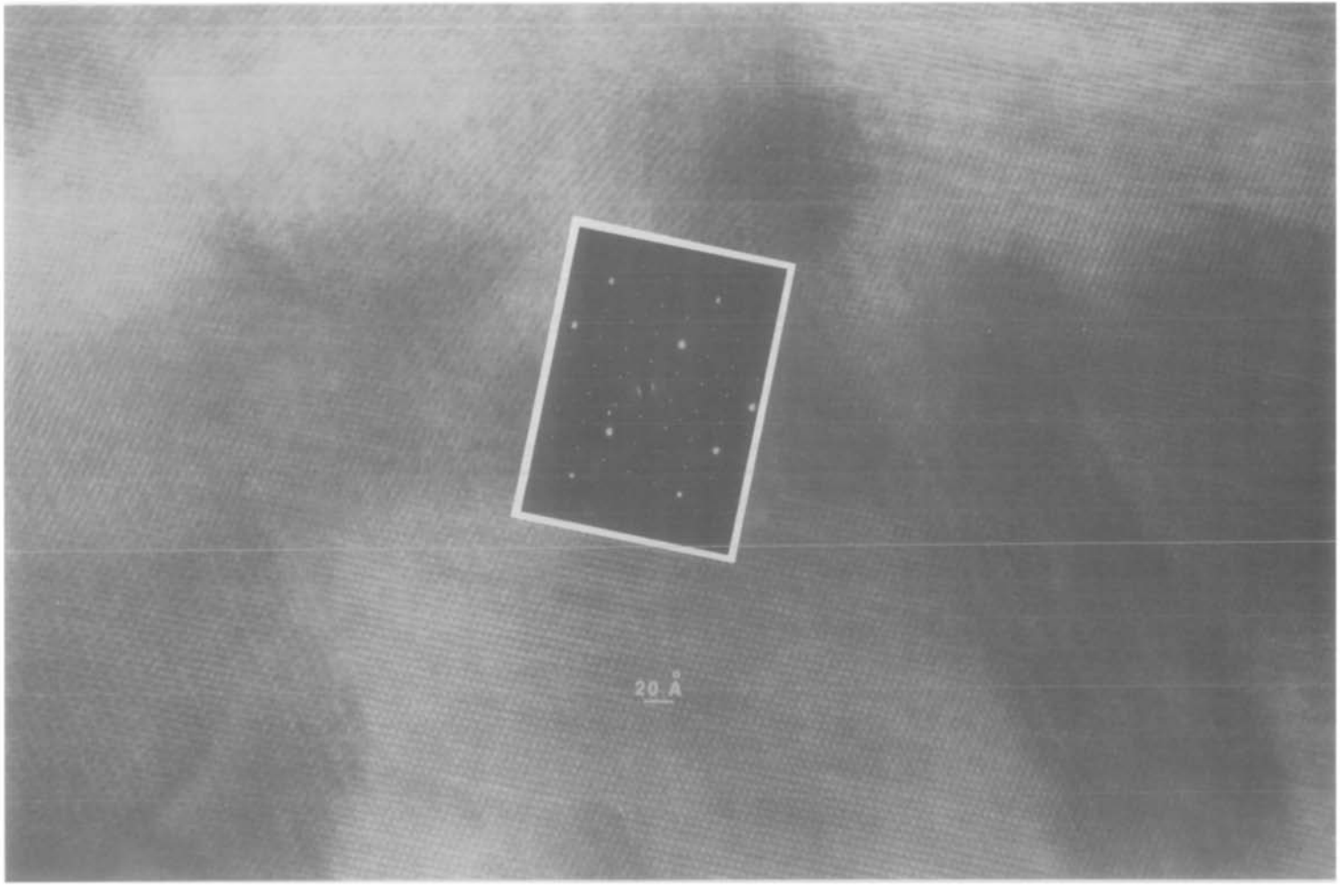

FIG. 5. A region of Pr_7O_{12} on which patches of Pr_2O_3 have begun to form, [21$\bar{1}$] zone. Notice the moiré patterns formed.

$[21\bar{1}]_F$ zone an analogous behavior is displayed. Figure 5 is an image of a crystal, largely Pr_7O_{12}, down the $[21\bar{1}]_F$ zone. Regions of quite different contrast may be seen over the surface of the crystal. These darker regions are characterized by having well-defined moiré fringes showing the perfect overgrowth of the ϕ phase on the underlying ι parent. Figure 6 shows the basis of the "beat" pattern of the two structures. Outlines of the projected unit cells are shown and the obvious pattern of register corresponding to the two types of regions can be seen. One set of fringes is along $(\bar{2}31)_\phi$, $(001)_\iota$ and the other along $(102)_\phi$, $(01\bar{1})_\iota$. These fix the observed register of the structure at four times the ι spacing along $(001)_\iota$ and $(0\bar{1}0)_\iota$.

The reduction of ι phase in this zone is obviously not uniform, but there is nucleation and growth in certain areas in what are probably very thin patches at this early stage of reduction. Further evidence that this is an early state is that the thin edge is not yet completely reduced. As reduction proceeded the ϕ phase continued to increase in intensity in the diffraction pattern with the appearance of double diffraction again when the two phases were of approximately equal intensity. Furthermore, there is a great deal of streaking in the diffraction pattern along $[0\bar{1}1]_\iota$, $[\bar{3}15]_\phi$ which appears as a general growth of ϕ irregularly on its $(10\bar{2})$ planes. The streaking shows a preference of four times the $(135)_F$ spacing (Fig. 5).

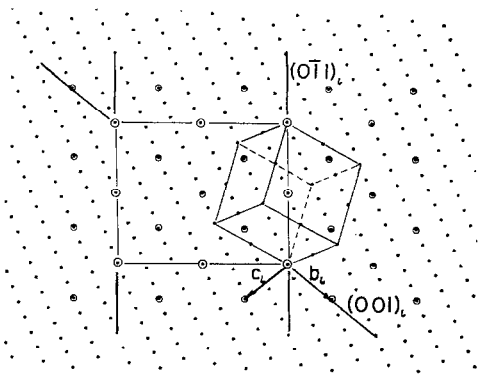

FIG. 6. A diagram showing the register of overlays of ϕ and ι phases. Dots mark columns of metal atoms in the $[211]_F$ zone of the fluorite substructure common to both phases. Open circles mark the projection of ι phase along its a axis in this zone. The projected cube outlines the ϕ phase in this zone. It has a volume eight times that of the fluorite subcell. The face-centered face of the subcell is one-fourth that of the ϕ cell face. The larger-sized open circles mark the positions of register of the ideal supercells. The directions of the solid lines outside the central rectangle mark directions of striations in the overlay ϕ–ι images.

The reduction of Tb_7O_{12} appears to proceed in much the same way as that of Pr_7O_{12}, although it has not been observed as frequently. A crystal of hydrothermally grown TbO_x with oxygen content greater than $TbO_{1.833}$ was heated in the electron beam of the microscope and successive images and diffraction patterns were taken. An interesting series was obtained in the $[111]_\phi$ zone as the crystal reduced incompletely from Tb_7O_{12} to Tb_2O_3.

Figure 7 illustrates a partially reduced ι phase. Notice a behavior quite analogous to that suggested for the Pr_6O_{11}–Pr_2O_3 reaction. Domains of ϕ approximately of the same size are intergrown coherently in a matrix of ι. At the thin edge (bottom right) of the crystal the domains have grown together more completely and they are further apart as the crystal becomes thicker. Although the cross-sectional areas of the domains vary by about a factor of 4, the absence of very small nuclei or nuclear cores is striking. Rather, there is some evidence at the region marked A in Fig. 7 of a *cooperative emergence* of ϕ in ι.

This suggests that oxygen is lost from the surface of the crystal from a substantial area (the nucleus is very shallow) followed by a cooperative rearrangement into domains of ϕ of approximately the same size. These domains are observed to grow laterally, in successive images, until impingement is complete. At the impingement in-

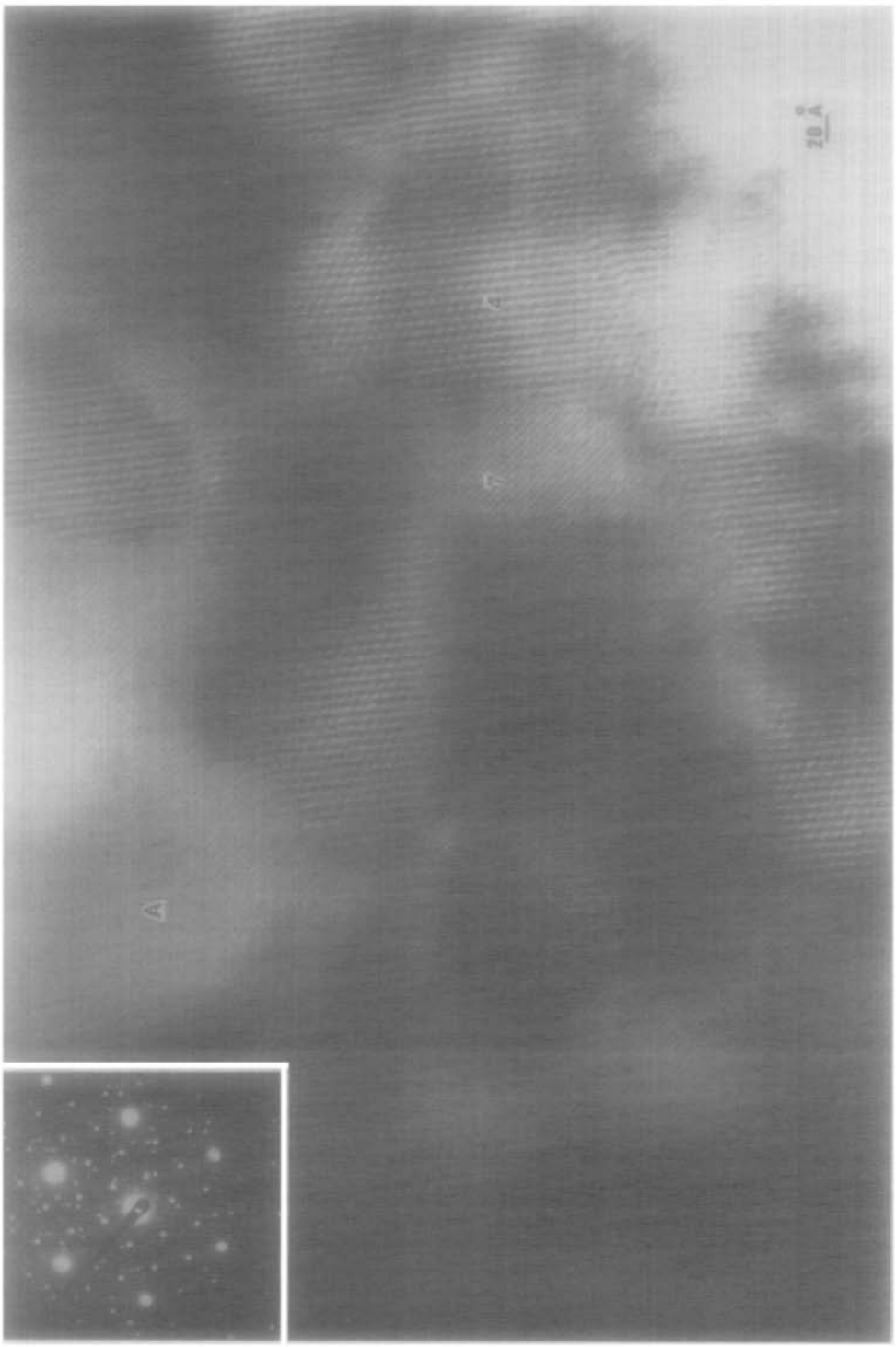

FIG. 7. The partial reduction of Tb_7O_{12} to Tb_2O_3, $[1\bar{1}1]_F$ zone. An emergent domain is marked by A, a developed domain of ϕ is marked by 4. The host is marked by 7.

terface there is the same lack of register of the ϕ domains, being offset by $\pm\frac{1}{4}$ and $\frac{1}{2}$ the inter-net spacing, and at the ϕ–ι interface register occurs at every fourth ι fringe. This behavior is entirely compatible with that of the reduction of Pr_7O_{12} described above (Fig. 4a).

Two other observations should be mentioned. (1) Structural disturbances at the ϕ–ι interface in all cases extend only a fraction of a unit cell, suggesting almost perfect coherence. (2) Hexagonal moiré nets resulting from an overlay of ϕ on ι phase are rare, suggesting that the penetration of the ϕ phase occurs rapidly and entirely through the crystal once the domain is formed.

The experience with specimens prepared and annealed in the composition range between ι and ϕ and then examined in the microscope was somewhat different. As mentioned above in the ZrO_2–Sc_2O_3 system, annealing produced macroscopic phase separation and crystals examined tended not to show interface regions (see Fig. 3). In the PrO_x system attempts were made to produce and observe diphasic samples in this composition region. While powder X-ray patterns of these annealed preparations were always diphasic, individual crystallites observed in the microscope were almost invariably either ι or ϕ (σ) only.

Diphasic electron diffraction patterns and images were obtained from only two crystals of the many observed. In Fig. 8 an ι–ϕ interface is seen in a PrO_x crystal. The C type has apparently formed from a single nucleus or from several with the fortuitous event of perfect register. In this case the two regions of the imaged crystal are relatively macrocrystalline and the interface reveals the same lack of register as in the radiation-induced reduction. Every fourth row of spots of the ι phase is in register with the ϕ phase. It should be noted that the obvious disturbance of the structure does not extend beyond one unit cell of either crystal in the interface.

The other diphasic case is illustrated in Fig. 9, which shows a $\langle 111\rangle_F$ lattice image of a σ-phase sample with an obvious fault. More importantly, the banded appearance perpendicular to the crystal edge is believed to result from a composition fluctuation of a σ-type phase. It is not yet clear whether these fluctuations reflect structurally different regions or only lattice parameters which fluctuate. This is the only case of coherent intergrowth of two "phases" observed in the composition interval $PrO_{1.5}$–$PrO_{1.714}$. The lack of such coherent intergrowth of ι and σ praseodymium oxides apparently results from their structural dissimilarity, underlining the fact that Pr_2O_3 is compositionally but not structurally $n = 4$ of the homologous series. The ability of the ι and ϕ phases to be semicoherent could result from the ability of the ϕ phase to accommodate a considerable composition variation and hence lattice parameter change, making the fluorite subcells nearly the same dimensions at the interface.

The Reduction of ζ (Pr_9O_{16}) to ϕ (Pr_2O_3) in the Electron Microscope

Many observations have been made of radiation-induced vacuum reduction of ζ-phase praseodymium oxide to the ϕ phase in the electron microscope. It is intended to imply that under strong radiation heating this reduction occurs without the appearance of the intermediate ι phase in the experiments to be described. In another paper the reduction of ζ to ι phase under milder conditions will be presented.

In the $[111]_F$ zone the growth plane common to both phases is most easily discerned. By application of the transformation matrices (6) the $[\bar{1}11]_F$ transforms into a $\langle\bar{1}10\rangle_\zeta$ and remains $[\bar{1}11]_\phi$. It is apparent that the direction $\langle 110\rangle_\zeta$—the plane in which oxygen vacancies are prevalent in the ζ phase—is common to that of $(110)_\phi$. Other low-index planes of the two cells form an angle with each other. It is also

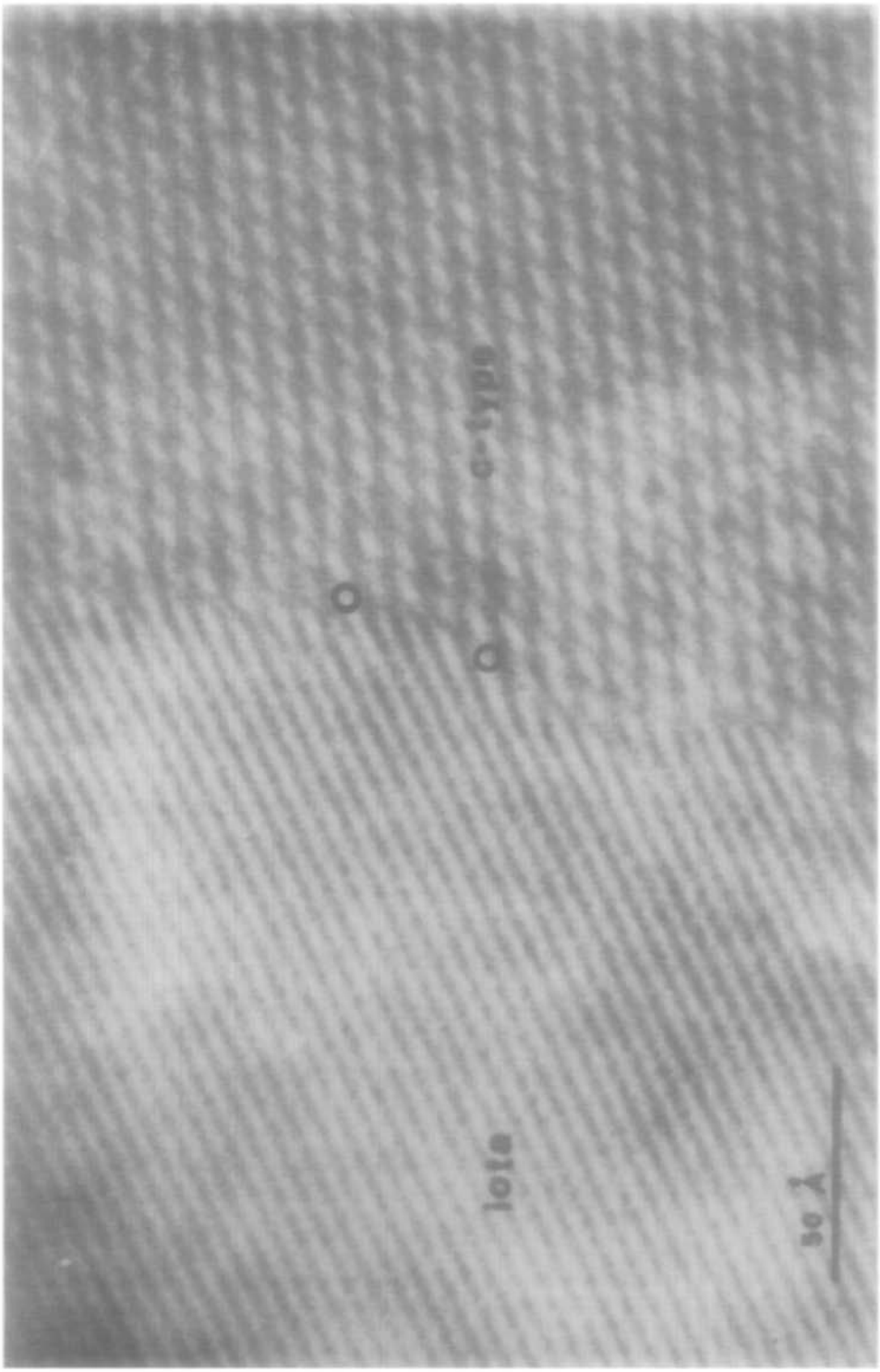

FIG. 8. An interface between ι and C-type phases. Notice the register between the two phases at every fourth ι fringe as suggested by the small circles, $[111]_\phi$ zone.

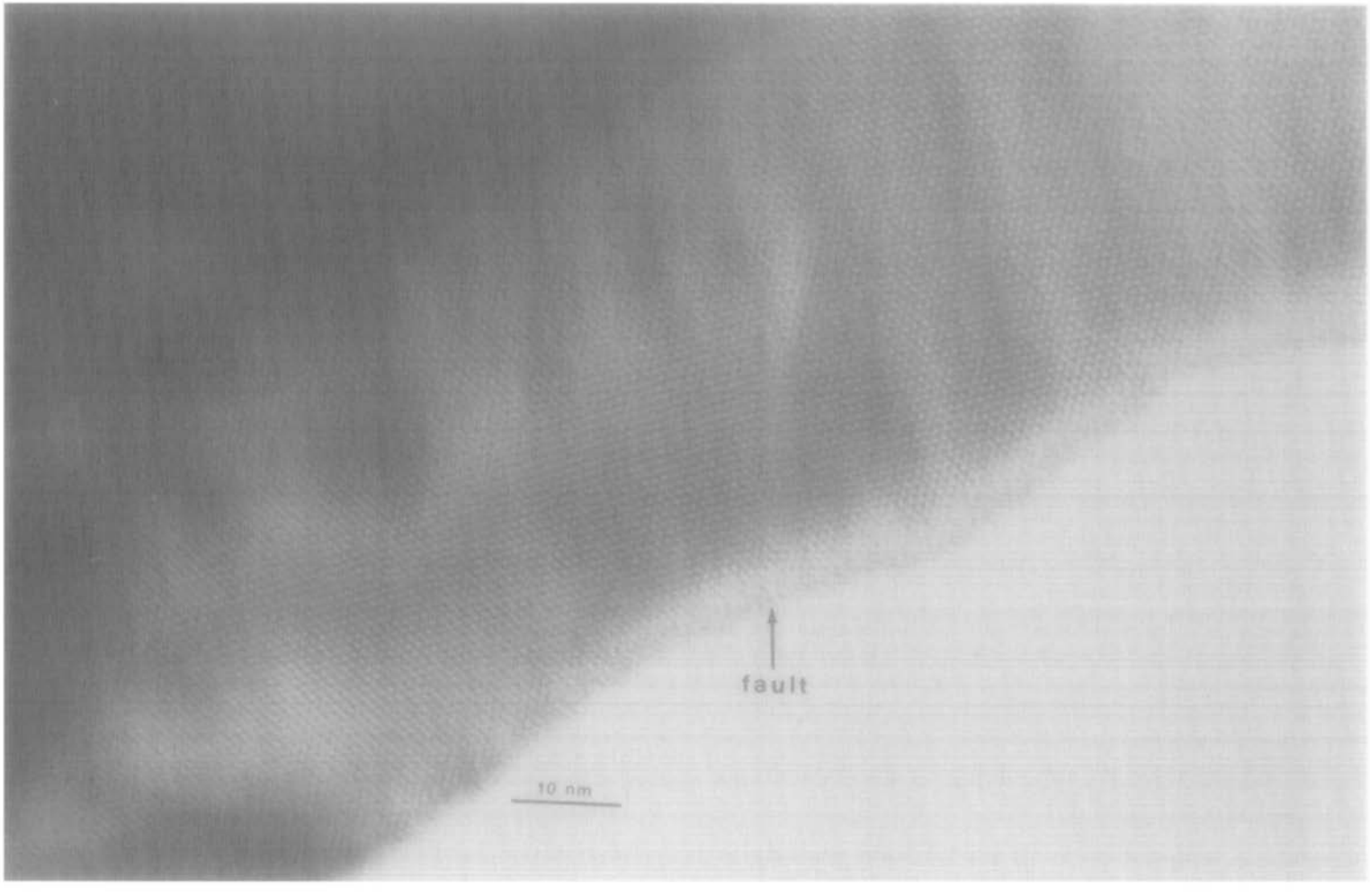

FIG. 9. An image, $[111]_F$ zone, of a crystal of σ-phase Pr_2O_{3+x}. Notice faulting and the banding, probably due to a composition modulation.

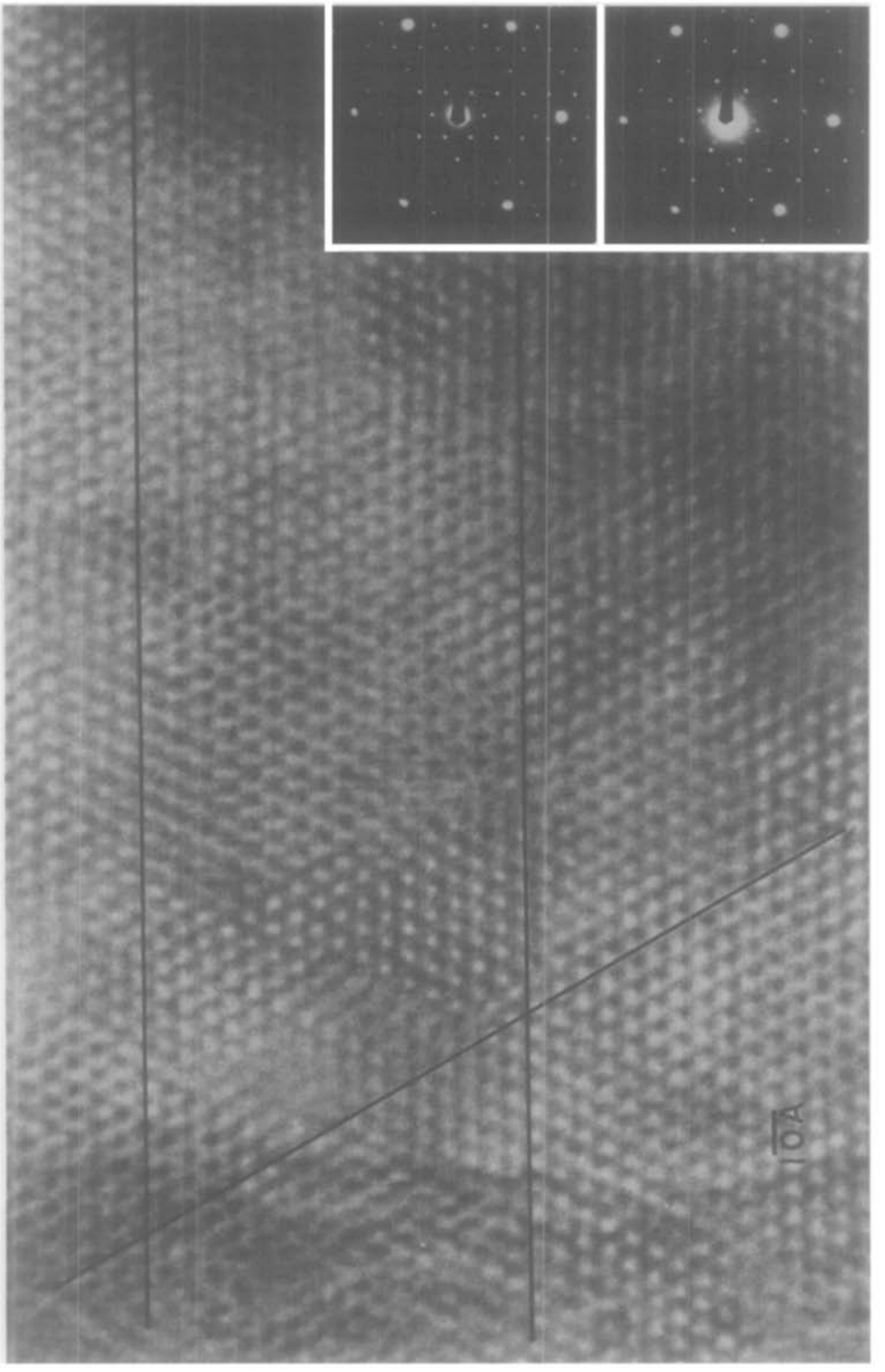

FIG. 10. An image of almost completely reduced ζ phase. Notice mismatched domains of ϕ phase emphasized by the lines drawn. Inset $[111]_F$ diffraction patterns before (bottom) and after (top) the image.

apparent that four ζ unit cells exactly register with three unit cells of ϕ.

The unannealed final reduction product as observed in the [111] zone is shown in Fig. 10. The hexagonal array of spots is typical of the images of the ϕ phase. In this case domains with triangular cross sections roughly about 100 Å in altitude form a mosaic with interfaces mismatched by $\pm\frac{1}{4}$ or $\frac{1}{2}$ of the inter-row spacings. This mismatch represents one or two metal atom row spacings in the fluorite substructure. The final product is very similar to that obtained when ι is reduced under similar conditions. In most cases the boundary transition is sharp, i.e., the domain interface boundaries have displaced spots only one or two atoms deep. But in a few instances curved rows suggest a less sharp transition. The interface compositions could differ significantly from that of the bulk sample.

Figure 11 diagrams a domain structure very similar to that observed. The background is the original ζ structure projected as small circles on the $[111]_F$ zone. The triangles represent the projection of the ϕ phase nucleated at random within ζ and growing until complete impingement occurs. The nuclei are more or less homogeneous over the area. This gives a mosaic quite similar to that observed where the nuclei would have been about 200 Å apart.

In one experiment, where the reaction ζ to ϕ had not proceeded very far, the micrograph showed well-crystallized ζ in the thicker regions of the crystal with substantial reduction to ϕ in the thinner parts and a good deal of irregular contrast with ϕ overlay in the intermediate regions. Figure 12 shows part of this intermediate region. In the upper left is a pattern of ζ phase only slightly modified. (Compare the contrast with the pattern of open circles in Fig. 11.) Further to the right the position and spacing of the spots is changing in a disordered way to the hexagonal pattern characteristic of the ϕ phase (the pattern of triangles of Fig. 11). Note that in the region marked A in Fig. 12 the pattern of the ϕ phase is quite clear for a few unit cells. Again, the irregular rows of spots which show the presence of ϕ on the right are clearly distinguishable

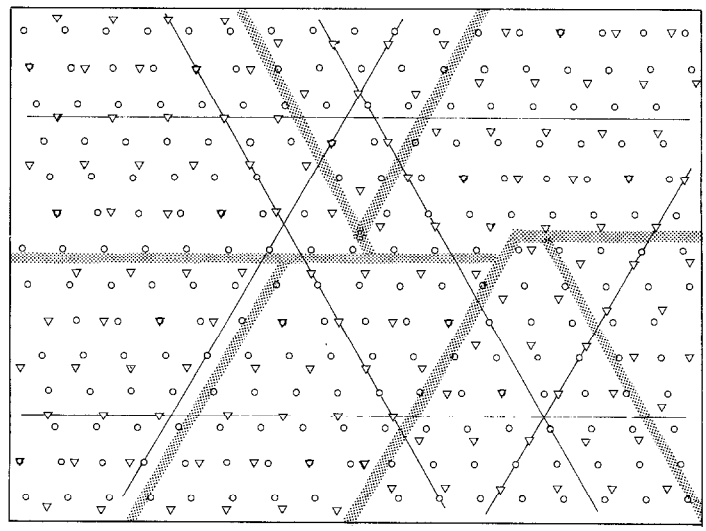

FIG. 11. An illustration of the consequences of random nucleation of ϕ in ζ phase with mismatched impingement, to be compared with Fig. 10. Circles mark the projection of the ζ phase and triangles that of ϕ. Dislocations of $\pm\frac{1}{4}$ or $\frac{1}{2}$ are emphasized by the drawn straight lines.

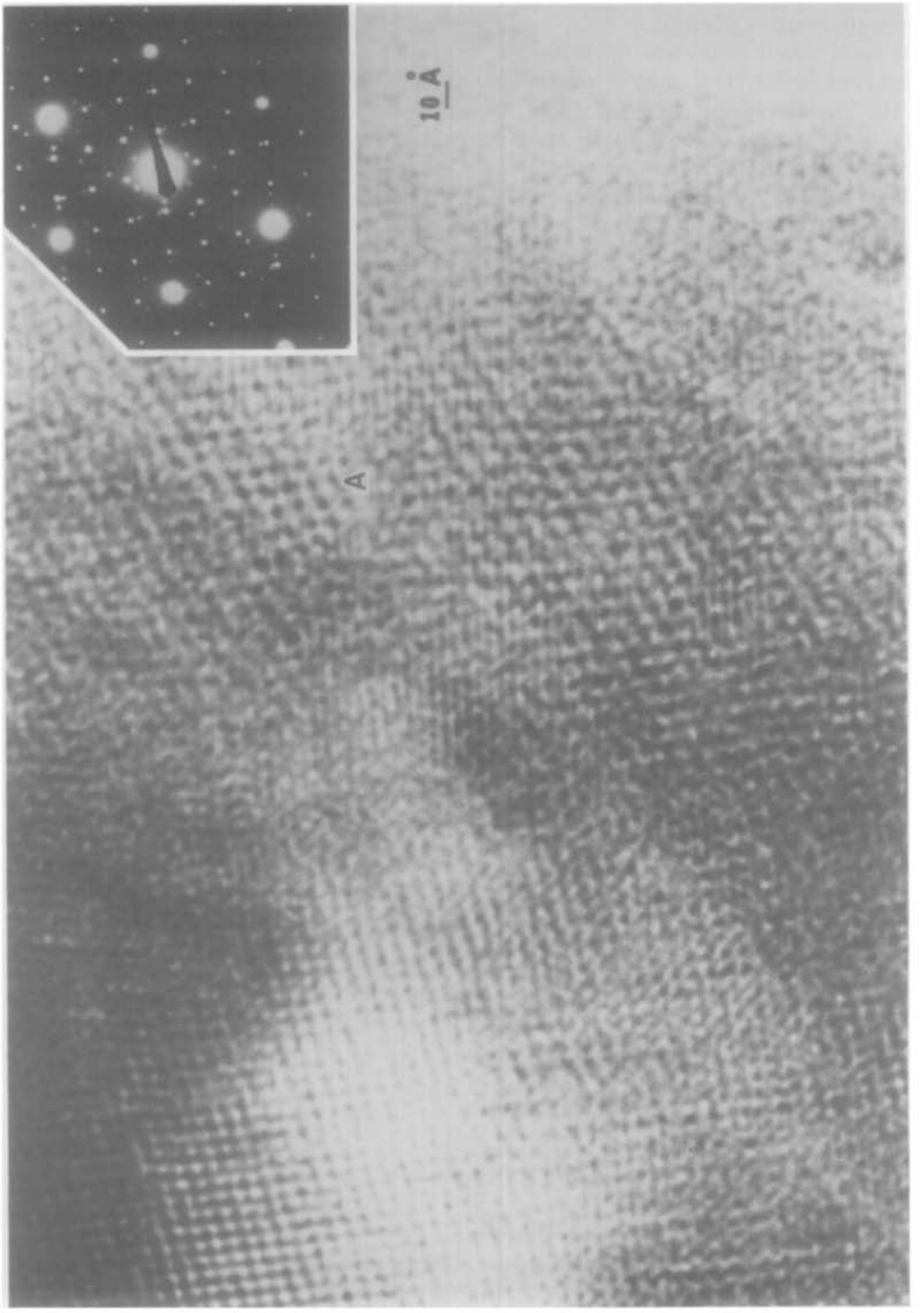

FIG. 12. The early stages of reduction of ζ to ϕ phase. The reaction is more obvious on the right, where A marks the hexagonal pattern of ϕ in this $[111]_F$ zone.

from those of ζ on the left side. The irregular appearance of the ζ pattern on the right is a relatively minor modulation due to ϕ, as is suggested again by viewing from right to left at low angle.

The same reaction has been observed in the $[21\bar{1}]_F$ zone with similar results. The relationship between the projections of the two phases in this zone is illustrated in Fig. 13, where it is clear that again there is a repeat of the same overlay condition every four ζ cells and there are four different origins possible. This gives rise to the wavy lines in the ϕ phase and the modulated appearance of the overlay regions seen in Fig. 14. Before that figure is discussed, a comment on the appearance of the ϕ phase along $[21\bar{1}]_F$ should be mentioned. Contrary to the appearance along $[111]_{\phi,F}$ where white dots in a hexagonal array occur, only fringes are observed in the $[21\bar{1}]_F$ zone for ϕ. This is because the $[21\bar{1}]_F$ direction in ϕ does not have the structural significance it has in either ζ or ι.

Figure 14 is an image and diffraction pattern of a phase, originally ζ, which is undergoing reduction in the microscope. In the thin edge at the lower left are seen the wavy

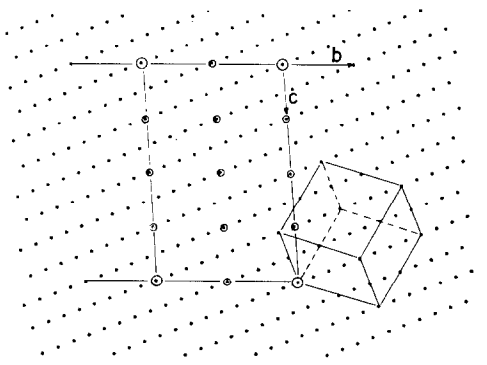

FIG. 13. A diagram showing the overlay pattern of ζ and ϕ phases. The small circles mark the projected unit cells of ζ and the cube of ϕ in the $[21\bar{1}]_F$ zone. The larger circles indicate the common dimensions of these unit cells and indicate the basis of striations in the images at the width of four unit cells of ζ, as are clearly seen in Figs. 14 and 15.

lines characteristic of a $[21\bar{1}]_F$ zone of ϕ phase when the source of the material is one of the higher oxides not annealed after formation. The waviness comes from the growing together of domains with a different core origin. Reaction is essentially complete in the thin edge.

In the wedge-shaped crystal where the thickness of the reactant and product are comparable, the pattern shows the modulation resulting from the overlay and origin shift which gives a beat frequency at four layers of Pr_9O_{16}. At the upper right-hand corner the effect of reduction is not very apparent and contrast due to ζ is dominating the image. The diffraction pattern at the lower right shows principally ζ phase with a small amount of ϕ.

Figure 15 shows one region of a crystal of ζ at different times as the reduction to ϕ is progressing. Note that reduction at the edge (the wavy fringes roughly parallel to the base) is just apparent in the left image but well developed on the right. The overlay responsible for a modulation of four layers of ζ is not apparent on the left but definitely shows up on the right. The diffraction pattern in the figure was taken after the second image and the original plate shows only the faintest spots due to the ϕ phase. Later patterns show the full development of the reduced phases.

As was mentioned above, under suitable conditions ζ phase reduces to ϕ via the well-characterized ι phase. In most of the many cases of which the figures shown are illustrations, the ϕ phase appeared to form directly without the agency of the ι phase. In a few cases, however, the ι phase did appear as a domain near the edge of the crystal. This marked departure from its formation from ζ to give intergrown planar inclusions of thin sections characteristic of the ζ–ι reaction suggests that it was formed by reoxidation of the ϕ phase by the diffusion of oxygen from the incompletely reduced bulk crystal, as discussed above.

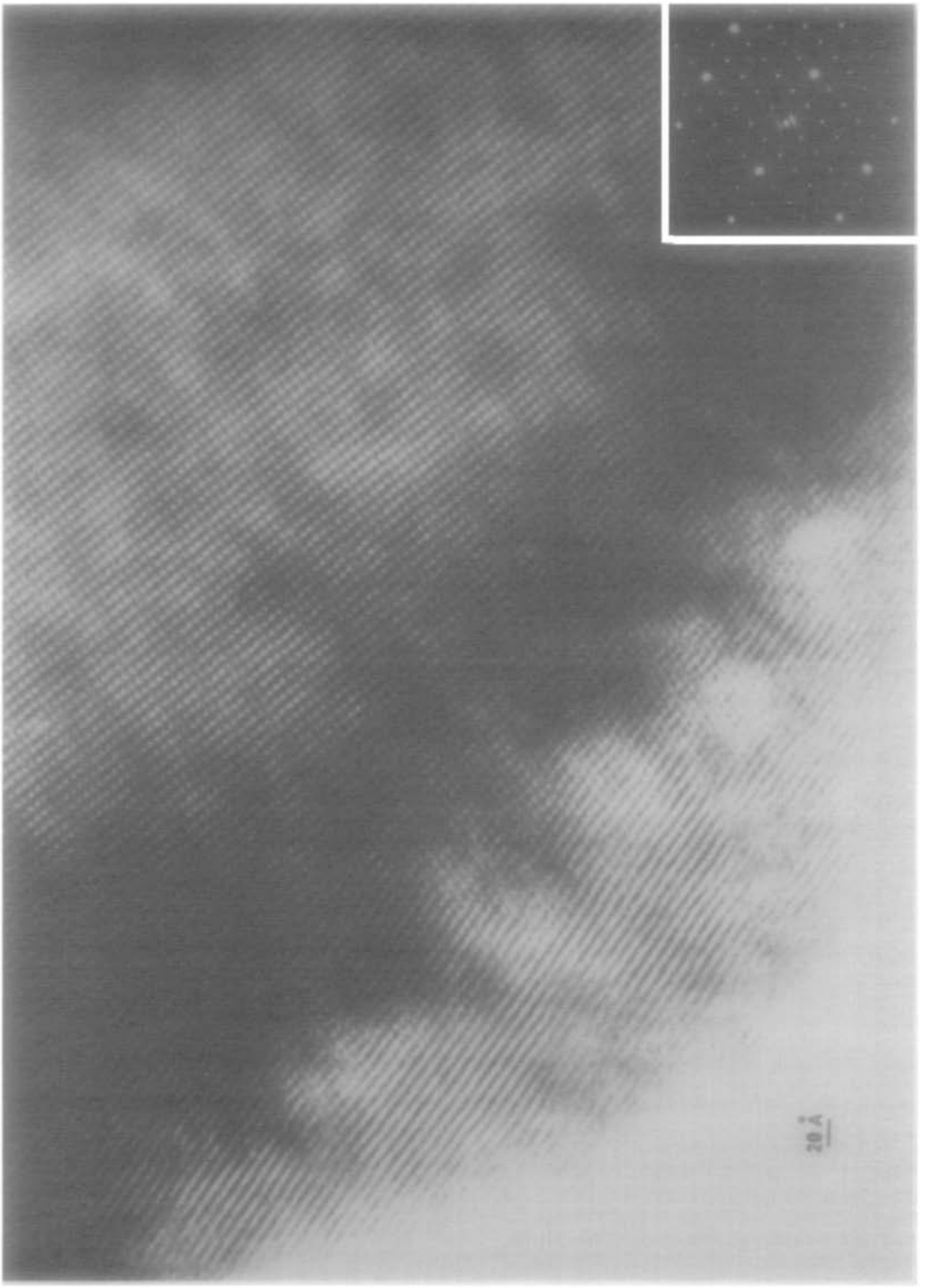

FIG. 14. A reduction of Pr_9O_{16} toward Pr_2O_3, $[22\bar{1}]_F$ zone. Reaction is nearly complete in the thin edge at the right. Striations indicate moiré fringes from overlay as indicated in Fig. 13.

The Occurrence of Disorder in Lattice Images

Apparent disorder is probably the rule rather than the exception in the lattice images obtained in this study. Figure 16 shows examples of disorder in $Zr_3Sc_4O_{12}$ arc-melted samples. Considering their thermal history, the occurrence of disorder in these samples is to be expected. It appears almost certain that it results from a nonuniform distribution of Zr^{4+} and Sc^{3+} ions which results in structural elements of adjacent phases being included in the sample. However, since this situation is highly metastable and an artifact of the preparation technique it could obviously be removed by annealing the sample.

Other examples of disorder in the PrO_x and TbO_x systems are common. Part of this disorder is probably a result of the examination techniques. As was previously mentioned, it is possible to both reduce and oxidize different parts of the sample at the same time, so there is little doubt that the observed extent of disorder is considerably greater than that of the equilibrium condition. Disorder is probably a prerequisite to reaction in these systems.

Conclusions

Higher oxides, specifically R_7O_{12} and Pr_9O_{16}, were observed to reduce in the vacuum of the electron microscope under electron irradiation. These samples were observed to pass through various stages until their compositions were near that of the end member of the series, R_2O_3. The transition (reaction) is reconstructive because, although the ϕ phase is compositionally a member of the homologous series R_nO_{2n-2}, and is fluorite related with metal atoms occupying essentially fluorite positions as in the higher oxides, the oxygen vacancy arrangement is profoundly different.

The sequence of events in this process may be summarized briefly as follows. The higher oxides show disorder, and nucleation of the ϕ phase appears to occur on the surface of the parent phase in what is termed "cooperative emergence." This term is meant to imply that a defect layer related to the product spreads on the surface in a premonitory way before rapid growth normal to the surface produces a domain of ϕ phase about 100 Å across. These domains appear to extend their boundaries until complete impingement occurs and a mosaic of domains reflects the random nucleation in the fluorite-related substructure. This behavior is confirmed by observing the reaction both in the $\langle 211 \rangle_F$ and the $\langle 111 \rangle_F$ zones.

The mosaic is semicoherent with evidence of stress accompanying the necessary mismatch. It is not known whether this behavior is a result of the fact that the specimens are very thin in one dimension or whether the same reaction occurs in bulk samples. Specimens prepared at equilibrium outside the microscope do not show this mosaic pattern in their ϕ-phase regions. It was also noted that the crystals of the materials annealed outside the microscope were usually unreacted or completely reacted with few hybrid crystals. This suggests that when nucleation does occur, reaction is rapid and complete and the mosaic pattern quickly anneals out if, indeed, the mechanism of reduction is the same. Grinding during specimen preparation for the microscope could also enhance the apparent phase separation by causing fracture along phase boundaries.

The observations on materials annealed outside the microscope are interesting when one remembers that there is a well-established intrinsic hysteresis in the phase reaction being observed which suggests a coherent intergrowth of domains of the new phase in the old which generally were not observed. Another possibility is that each crystallite has its own free-energy surface and transforms under conditions dictated

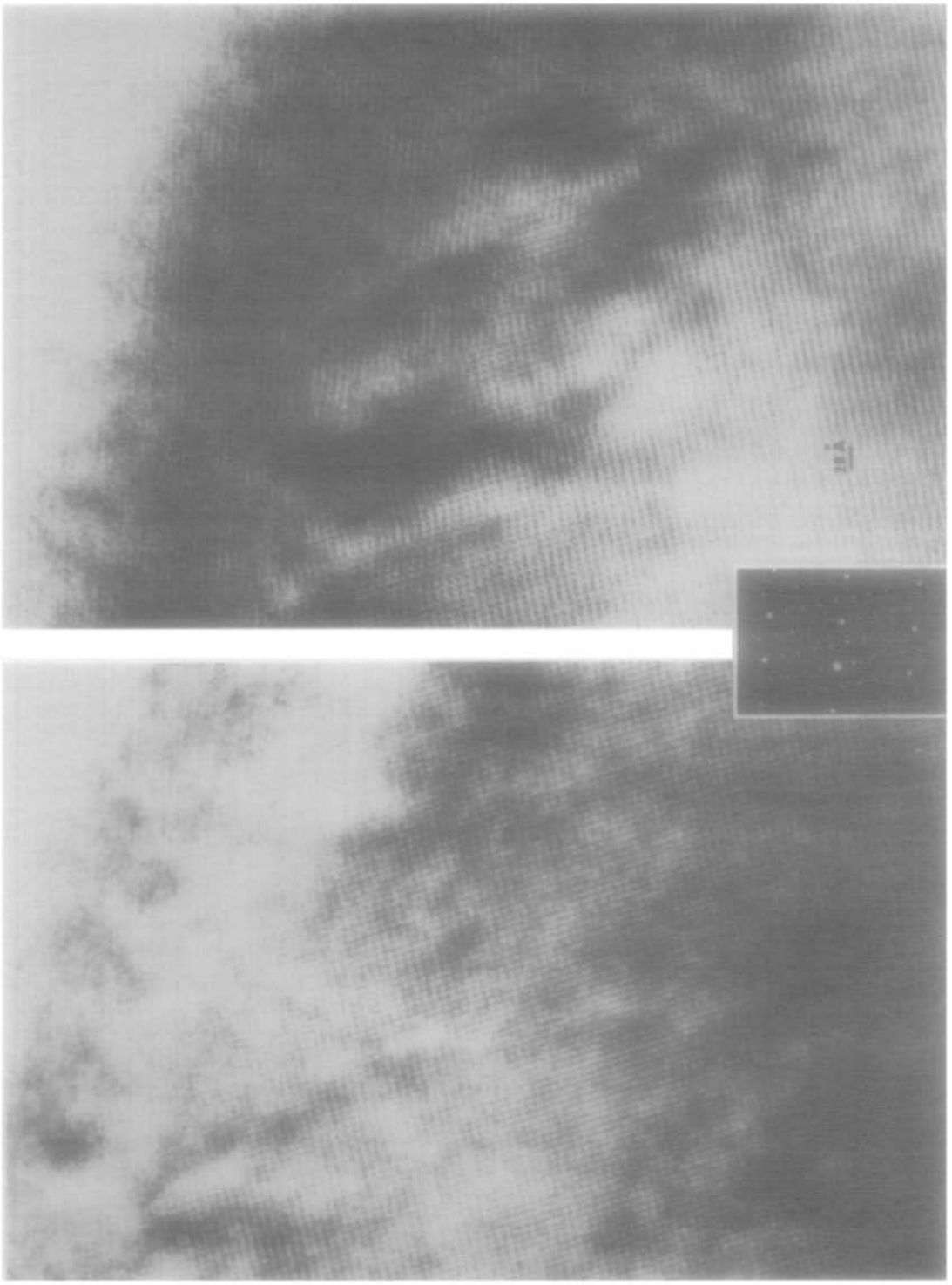

FIG. 15. Two stages of reduction of the same area of a ζ-phase crystal in the $[21\bar{1}]_P$ zone.

by its state and the changing ambience. Once the reaction begins it proceeds rapidly to completion. If the same applies to powdered particles the reproducible hysteresis would be seen to result from the "average" behavior of the specimen. The reaction sequence for any one particle would be unpredictable but, in aggregate, perfectly reproducible, much as a gas-phase distribution of molecules obey some gas law. The effect of domain-size distribution on hysteresis has recently been considered in the rare earth oxide systems (*15*).

The pseudobinary system $Zr_ySc_{1-y}O_x$ behaves in a way that would be expected from the above experiments, that is, as a binary rare earth oxide in this same composition region if held at constant composition after some initial reduction. When annealed, the initial matrix of small domains suffered a massive phase separation.

We speculate now on some details of the reactions observed and implied. Reduction appears first in the thinner parts of the crystal. This may be a reflection of the greater sensitivity of the technique to the presence of a new phase in only a few layers of the parent material. In all probability the reduced phase is nucleated in the surface cooperatively and spreads both outward and inward as the reaction progresses. Evidence for surface growth comes from the irregular striations which emanate from the ϕ area into the oxidized reactant region. These striations probably result from double diffraction. The original beam diffracted first by the epitaxial surface-reduced layer is then diffracted again when it encounters the parent phase. Since the unit cells of the epitaxial phase and the parent phase are at an angle to each other, and since the thickness of each phase is changing (one increasing while the other is decreasing), it seems likely that certain thicknesses can combine with the angular difference to produce the striations.

The striations which exhibit a repeat pattern of four fringes of the parent material along $(110)_\zeta$ and $(111)_\phi$ have a different origin. Figures 6 and 14 show the regular register of the overlay of ϕ and either ι or ζ phase at spacings of four unit cells of the latter two. This repetition pattern could provide beam reinforcement along the common overlap direction, as is clearly observed. These observations suggest certain features caused by an epitaxial intergrowth of the reactant and product but gives no information on their spatial disposition (i.e., whether on or in).

Although these features are consistent with a surface layer of product phase, they do not prove the mechanism. The ϕ phase might start at the edge and grow into the center of the parent. Such a mechanism would be unlikely, however, in view of the gradient of the oxygen chemical potential, which increases with the depth of the crystal. Clearly, with the ζ phase, growth of a reduced phase within the interior would be expected to be a coherent ι phase rather than ϕ. The oxygen potential in the interior would be thermodynamically unfavorable for the formation of ϕ phase.

In addition, the change of volume associated with the reduction process argues against the growth of ϕ in the interior of either ζ or ι phases. From the lattice parameters (*6*) the volume of a unit cell of the ζ phase is 336.7 Å^3. The volume of the ϕ phase is 1356.6 Å^3. The ϕ phase unit cell has eight fluorite subcells and the ζ $\frac{9}{4}$ of these. From this one calculates a 13% volume increase as reduction occurs. Furthermore, since the ζ and ϕ phases match along their (110) planes, one can calculate the linear increase expected perpendicular to (110). For ζ, $d_{(110)} = 4.49$ Å, while for ϕ, $d_{(110)'} = 7.886$ Å [$d_{(110)}(\sigma) = 7.828$ Å]. Since four cells of ζ must match, at a minimum, three cells of σ, the corresponding distance is 19.8 vs 23.5 Å, a difference of about 19%. This large increase, both in volume and in linear dimension, would result in a severe

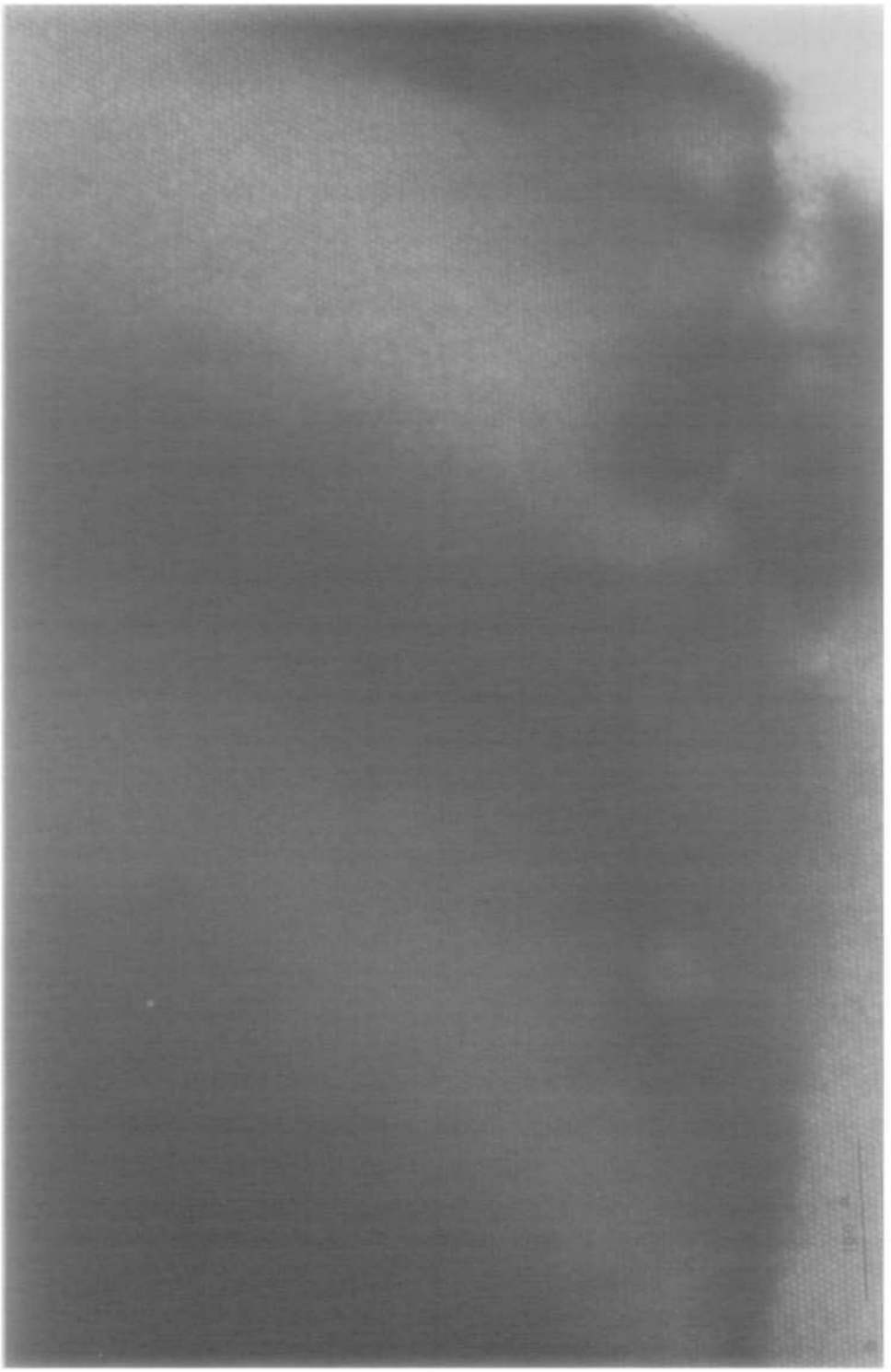

FIG. 16a. Disorder evident in $[111]_F$ zone image of $Zr_3Sc_4O_{12}$.

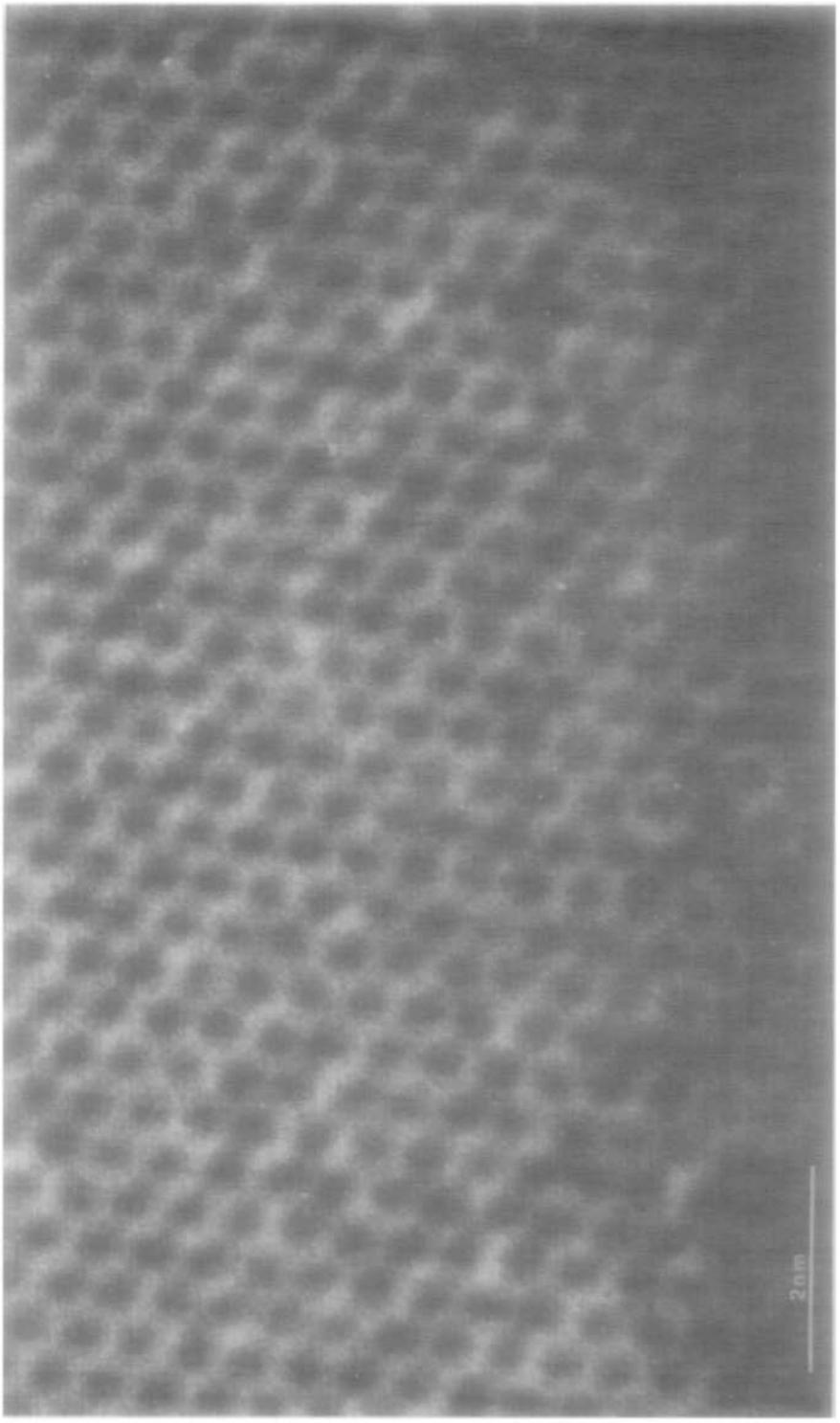

FIG. 16b. Disorder evident in $[111]_F$ zone image of $Zr_3Sc_4O_{12}$.

internal pressure and would mitigate against reduction occurring in the interior of a higher oxide crystal. Indeed, it is most likely that the ϕ (or σ) phase must grow on the surface so that another dimension is available to allow for the great volume change.

In comparison, the ι phase has a volume of 293.7 Å^3 and $\frac{7}{4}$ fluorite cells—giving a 1% change for ζ but a 3.3% change for the ϕ phase. In contrast the volume change in going from PrO_2 to Pr_2O_3 is only 11%.

In the ι phase, striations again run parallel to (001) typically four unit cells apart. Some striations are parallel to $(0\bar{1}1)$. In this direction there is a match every other cell.

Acknowledgments

The hydrothermally grown crystals were provided by Michael McKelvy. John Wheatley maintained the microscope facility. Helpful discussions were had with John Cowley and Sumio Iijima. Financial support was from NSF Grants DMR 77-08473 and 80-06584. Help was also provided by NSF Grant CHE-7916098 (The Regional Instrumentation Center for High Resolution Electron Microscopy). For all this support and encouragement we are most grateful.

References

1. J. M. COWLEY, *Annu. Rev. Mater. Sci.* **6,** 53 (1976).
2. L. EYRING, *in* "Solid State Chemistry: A Contemporary Overview" (S. M. Holt, J. B. Milstein, and M. Robbins, Eds.), Paper 2, p. 27, Advances in Chemistry Series 186, American Chemical Society, Washington, D.C. (1980).
3. L. EYRING, *in* "Nonstoichiometric Oxides" (O. T. Sørensen, Ed.), pp. 337–398, Academic Press, New York (1981)
4. A. J. SKARNULIS, E. SUMMERVILLE, AND L. EYRING, *J. Solid State Chem.* **23,** 59 (1978).
5. M. A. O'KEEFFE, P. R. BUSECK, AND S. IIJIMA, *Nature (London)* **274,** 322 (1978).
6. P. KUNZMANN AND L. EYRING, *J. Solid State Chem.* **14,** 229 (1975).
7. E. SUMMERVILLE, R. T. TUENGE, AND L. EYRING, *J. Solid State Chem.* **24,** 21 (1978).
8. R. T. TUENGE AND L. EYRING, *J. Solid State Chem.* **29,** 165 (1979).
9. R. T. TUENGE AND L. EYRING, *J. Solid State Chem.* **41,** 75–89 (1982).
10. G. SCHIFFMACHER, *J. Microsc. Spectrosc. Electron.* **2,** 503 (1977).
11. M. Z. LOWENSTEIN, L. KIHLBORG, K. H. LAU, J. M. HASCHKE, AND L. ERYING, *in* "Proc., NBS Inst. for Mater. Res., 5th Mater. Res. Symp., Gaithersburg, Md., October 18–21, 1971," *NBS Spec. Publ. (U.S.)* **364,** 343 (1972).
12. S. IIJIMA, *Acta Crystallogr. Sect. A* **29,** 18 (1973).
13. M. R. THORNBER, D. J. M. BEVAN, AND J. GRAHAM, *Acta Crystallogr. Sect. B* **24,** 1183 (1968).
14. D. J. M. BEVAN AND E. SUMMERVILLE, *in* "Handbook on the Physics and Chemistry of Rare Earths" (K. A. Gschneidner, Jr., and L. Eyring, Eds.), Vol. III, pp. 437–438, North-Holland Publishing Company, Amsterdam (1979).
15. S. H. LIN, M. B. LANGLEY, R. H. LANGLEY, AND L. EYRING, to be published.